

See discussions, stats, and author profiles for this publication at: <https://www.researchgate.net/publication/276277573>

New Dimeric Carbazole–Benzimidazole Mixed Ligands for the Stabilization of Human Telomeric G-Quadruplex DNA and as Telomerase Inhibitors. Remarkable Influence of Spacer

ARTICLE *in* ORGANIC & BIOMOLECULAR CHEMISTRY · MAY 2015

Impact Factor: 3.56 · DOI: 10.1039/C5OB00675A

READS

47

4 AUTHORS, INCLUDING:



[Basudeb Maji](#)

Harvard Medical School

12 PUBLICATIONS 135 CITATIONS

[SEE PROFILE](#)



[Santanu Bhattacharya](#)

Indian Institute of Science

236 PUBLICATIONS 6,515 CITATIONS

[SEE PROFILE](#)



Cite this: *Org. Biomol. Chem.*, 2015,
13, 8335

New dimeric carbazole–benzimidazole mixed ligands for the stabilization of human telomeric G-quadruplex DNA and as telomerase inhibitors. A remarkable influence of the spacer†

Basudeb Maji,^a Krishan Kumar,^a K. Muniyappa^b and Santanu Bhattacharya^{*a,c}

The development of G-quadruplex (G4) DNA binding small molecules has become an important strategy for selectively targeting cancer cells. Herein, we report the design and evolution of a new kind of carbazole-based benzimidazole dimers for their efficient telomerase inhibition activity. Spectroscopic titrations reveal the ligands high affinity toward the G4 DNA with significantly higher selectivity over duplex-DNA. The electrophoretic mobility shift assay shows that the ligands efficiently promote the formation of G4 DNA even at a lower concentration of the stabilizing K⁺ ions. The TRAP-LIG assay demonstrates the ligand's potential telomerase inhibition activity and also establishes that the activity proceeds via G4 DNA stabilization. An efficient nuclear internalization of the ligands in several common cancer cells (HeLa, HT1080, and A549) also enabled differentiation between normal HFF cells in co-cultures of cancer and normal ones. The ligands induce significant apoptotic response and antiproliferative activity toward cancer cells selectively when compared to the normal cells.

Received 5th April 2015,

Accepted 13th May 2015

DOI: 10.1039/c5ob00675a

www.rsc.org/obc

Introduction

The telomere plays an important role in chromosomal protection, genomic stabilization, and cellular ageing.¹ A telomere in mammalian cells consists of a tandem repeat of the guanine-rich hexameric (5'-TTAGGG-3') sequences even up to 5–15 kb lengths from the extreme 3'-end. The single-stranded overhang is susceptible to degradation through different cellular mechanisms.² To protect the telomeric end, the cell adopts certain protecting mechanisms like end-capping and T/D-loop formation in the presence of a few telomere binding proteins.³ During chromosomal duplication, the extreme end of the telomere cannot be copied due to the presence of Okazaki fragments, known as the 'end-replication problem'.⁴ Thus, upon every cell division, the telomere length decreases, and when it reaches a critical length, it promotes genomic instability eventually leading to cell cycle arrest through 'end-to-end fusion'.⁵ To overcome the genomic problem, cells sometimes over-

express the telomere repairing protein telomerase, even up to 85–90%.⁶ Telomerase maintains the telomere length by adding repetitive nucleotides through the reverse transcriptase mechanism using its own RNA template present in the hTR (human telomerase RNA) component. The up-regulation of the telomere by the overexpressed telomerase maintains the overhang throughout the generations leading to an uncontrolled proliferation.⁷ However, there is hardly any evidence of the detection of telomerase in most somatic cells.⁶ Thus, the presence of overexpressed telomerase only in cancer cells offers a platform to discriminate them from the normal somatic cells. Consequently, an effective inhibition of telomerase activity is a viable strategy for the design and synthesis of an anticancer agent.

Unlike the duplex DNA which exists essentially throughout the genome, the telomeric G4 DNA emerges from the single-stranded 3'-overhang in the telomere. The biological importance of the G4 DNA was revealed when the G4 DNA mediated telomerase inhibition was invented.⁸ Telomerase, which acts only on the single-stranded DNA overhang, was found to be totally inactive upon folding into secondary tetraplex structures like the G-quadruplex. The design of ligands which can stabilize and significantly shift the equilibrium toward the G4 DNA structure and thereby inhibit telomere recognition has become a popular and promising strategy in oncology.^{9–11} It should be noted that ligands with poor discrimination ability between the duplex and the G-quadruplex DNA may result in

^aDepartment of Organic Chemistry, Indian Institute of Science, Bangalore 560 012, India. E-mail: sb@orgchem.iisc.ernet.in; Fax: (+91) 80-2360 0529;

Tel: (+91)-80-2293 2664

^bDepartment of Biochemistry, Indian Institute of Science, Bangalore 560 012, India

^cJawaharlal Nehru Centre for Advanced Scientific Research, Bangalore, Jakkur 560 064, India

† Electronic supplementary information (ESI) available: For additional synthetic procedure, characterization, spectroscopic data, cellular data, computational and experimental methods. See DOI: 10.1039/c5ob00675a

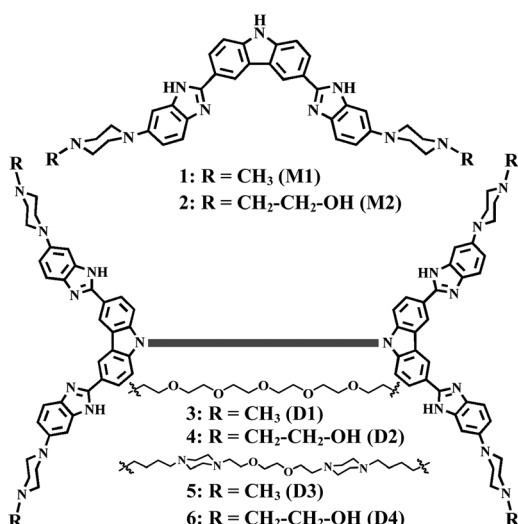


Fig. 1 Molecular structures of the ligands used in the investigation.

undesirable cytotoxic events which are considered as the side effects in DNA targeted chemotherapy. Thus, the development of efficient G4 DNA binding molecules with high selectivity over the double-stranded DNA is of keen interest to achieve desirable chemotherapeutic outcomes.^{12,13}

Herein, we introduce six novel carbazole based benzimidazole derivatives which contain two monomers, and the other four are dimeric molecules having different types of linkers that connect the individual monomeric units (Fig. 1). Each new ligand was examined toward its G4 DNA binding efficiency using different spectroscopic, electrophoretic, enzymatic, and cellular studies. Finally the nature of DNA-ligand interactions was further investigated with the help of molecular modelling studies. All the ligands showed high G4 DNA binding affinity with significant selectivity over the duplex DNA. The ligands also demonstrated potential telomerase inhibition ability and cancer cell selective toxicity. Importantly, the dimeric ligands demonstrated a significantly high G4 DNA binding and stabilization capacity compared to their monomeric counterparts, and their activity is found to rely considerably on the nature of the linker chain.

Results and discussion

Considerations in the ligand

Recently, there has been significant progress in the molecular design of synthetic benzimidazole based systems for the switchover of nucleic acid recognition from the duplex to the G4 DNA.¹⁴ Benzimidazole based Hoechst molecules were developed a long time ago, which have been utilized extensively to target the duplex DNA through the minor groove.¹⁵ Thereafter, efforts have been directed toward the structural modifications to enable their selective targeting of higher order DNA structures like the G-quadruplex. For instance, benzimidazoles

linked with one central aromatic ring, like a phenyl or pyridine moiety have been demonstrated for their preferential G-quadruplex DNA binding properties.^{16,17} Recently, it has been revealed that the replacement of the mono-nuclear aromatic ring with extended planar scaffolds like tri-nuclear heteroaromatic moieties, *e.g.*, carbazole, phenanthroline, *etc.* enhances the potential of the resulting ligands significantly toward the G-quadruplex DNA.^{18,19} The carbazoles and bis-benzimidazoles on their own have also been reported to show significant biological activities including cell permeability.^{20–22} Therefore, we have chosen new ligands based on a benzimidazole–carbazole mixed core.

Another substantial advancement in the ligand design strategy was reported *via* the use of dimeric forms of ligands.^{23–29} In particular, the dimeric ligands derived from 1,3-phenylene-bis-benzimidazole containing suitable spacers were distinctly superior compared to their corresponding monomeric forms in terms of their G4 DNA binding affinity, thermal stability, and telomerase inhibition activities.²⁹ Interestingly, the activity of the dimeric ligands was also reported to be highly dependent on the spacer length where ligands with a hexaethylene glycol type spacer showed the maximal activity among all the ligands studied in the series. To date, only a couple of other reports on the dimeric G4-ligands have been identified, in which the dimers based on acridine, quinoacridine, BRACO19, and macrocyclic hexaoxazoles show quite promising potential toward clinical applications.^{23–29} These reports reveal the importance of the dimeric ligands in terms of their substantially higher activity than their monomeric counterparts. Moreover, the reports also emphasize the significance of the length of the linker and its chemical nature in the ligand's solubility, affinity, and selectivity over other relevant DNA structures.^{23–29} The activity of the dimeric ligands was found to be highly dependent on the spacer length. It has been observed that the length of the spacer should be optimal so that the two binding moieties can efficiently interact with their preferable binding sites. Moreover, incorporation of a long hydrophobic methylene based spacer may actually decrease the ligand's activity while the oxyethylene based spacer shows higher water solubility and enhanced DNA binding activity.^{23–29} Thus, the design of dimeric ligands targeting the G4 DNA is worthwhile in the development of potential anticancer drugs for the future (ESI, Fig. S1†).

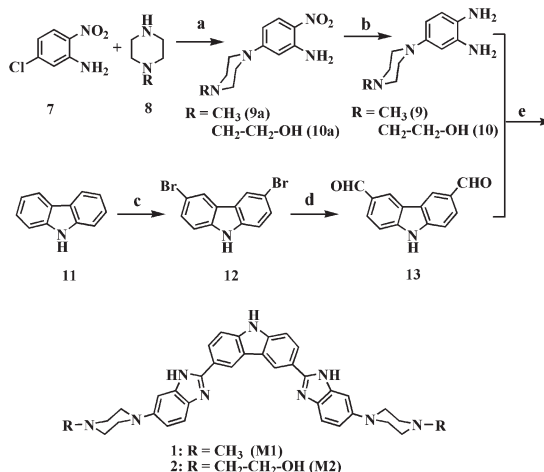
Based on the rationale presented above, we have synthesized a series of ligands having a carbazole core inserted between two benzimidazole units to form symmetric, planar pharmacophores with two piperazine moieties at the termini. The resulting ligands should bind DNA efficiently *via* stacking as well as H-bonding interactions whereas the end piperazine moieties in them should exist in their protonated forms at physiological pH to offer favorable electrostatic interactions with the DNA.

It is always a challenging task to specifically target G4 DNA over the predominant DNA form like duplex DNA. The duplex DNA binder ligand Hoechst 33258 has a characteristic crescent-shape with a concave interacting surface of

~145° (ESI, Fig. S1A†). To minimize the duplex DNA affinity, the present set of ligands was engineered with a significantly higher angularity of ~100° (ESI, Fig. S1B†) which can not only ‘discourage’ the Hoechst-like ds-DNA minor groove binding interaction but may also render the molecular shape favorable toward the dimension of a G-tetrad (ESI, Fig. S1D†). The similarity in the dimensions of the ligand and that of the G-tetrad predicts a favorable π-stacking interaction between the comparatively smaller Watson–Crick base pairs present in the duplex DNA (ESI, Fig. S1C and D†). Taken together, these new molecules should possess not only adequate affinity toward the G4 DNA but also significant selectivity over the duplex DNA.

Two monomeric molecules **1** (**M1**) and **2** (**M2**) having free carbazole-*N* core were synthesized. The corresponding dimeric molecules (**D1**, **D2**, **D3**, and **D4**) possess two different types of spacers that connect the ‘monomers’ *via* two carbazole-*N* ends (ESI, Fig. S2†). Following the previous reports on the design of dimeric molecules, a hexaethylene glycol based spacer was chosen since it demonstrated better efficiency toward G4 DNA stabilization compared to its monomeric counterparts. On the other hand, we have also investigated the effect of insertion of piperazine in the spacer. It may be noted that the hexaethylene glycol based spacer serves as a neutral spacer in the dimeric ligands while the linker having piperazine moieties provides additional sites of possible protonation at physiological pH.

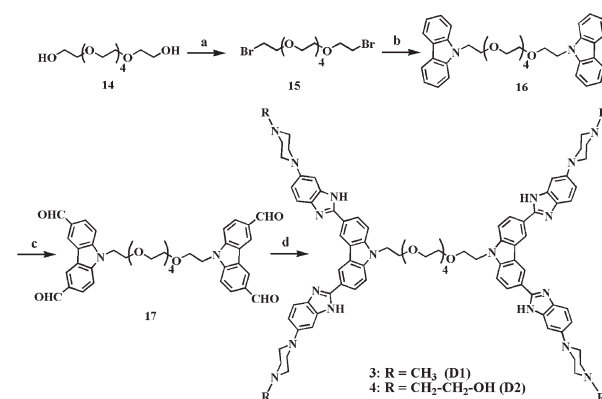
Initially, upon reaction with NBS, carbazole was converted to 3,6-dibromocarbazole (**12**) which was transformed following a reported procedure³⁰ in the presence of *n*-BuLi to obtain the 3,6-diformyl carbazole (**13**). The dialdehyde (**13**) was then coupled with two different types of freshly prepared diamines (**9** or **10**) to afford the corresponding benzimidazole derivatives



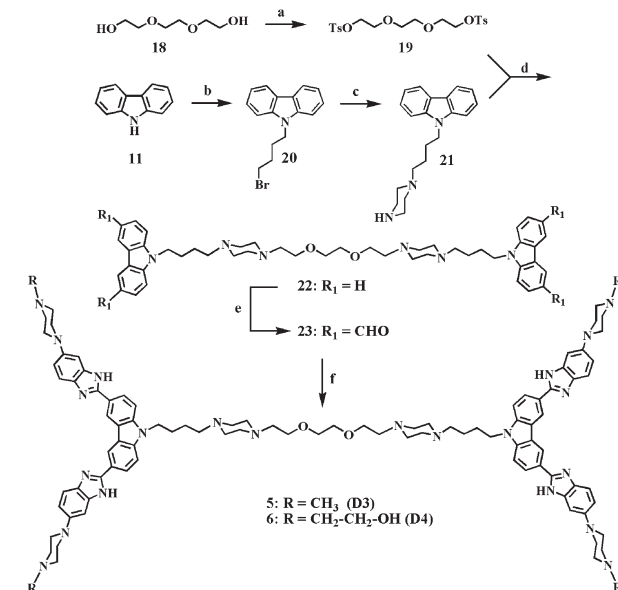
Scheme 1 Reagents, conditions and yield. (a) K_2CO_3 , dry DMF, 110 °C, 24 h, 89%; (b) $Pd/C-H_2$, EtOH, rt, 24 h, 100%; (c) NaH , NBS, dry DMF, rt, 6 h, 85%; (d) (i) KH , THF, 0 °C, (ii) n -BuLi, -78 °C → 25 °C, (iii) DMF, -78 °C → 25 °C, (iv) 1 M H_3PO_4 , 27%; (e) 4-(4-methylpiperazin-1-yl)-benzene-1,2-diamine (9) or 2-(4-(3,4-diaminophenyl)piperazin-1-yl)ethanol (10), $Na_2S_2O_5$, EtOH, 80 °C, 12 h, 55–65%.

1 (**M1**) and **2** (**M2**) through $Na_2S_2O_5$ mediated oxidative cyclizations (Scheme 1).¹⁶

The monomers (**1** and **2**) were then individually joined with each other *via* two different kinds of linkers, one having a neutral hexaethylene glycol based unit and the other having both oxyethylene and protonatable piperazine moieties in between such a spacer to furnish the dimeric molecules **3** (**D1**), **4** (**D2**), **5** (**D3**), and **6** (**D4**) respectively (Schemes 2 and 3). All the new compounds as well as their reaction intermediates



Scheme 2 Reagents, conditions and yield. (a) PPh_3 , Br_2 , acetonitrile, 0 °C → rt, 48 h, 70%; (b) carbazole, TBAI (cat.), 50% $NaOH$, $THF-H_2O$, 24 h, 55%; (c) $POCl_3$ -DMF, $ZnCl_2$, 110 °C, 24 h, 65%. (d) 4-(4-Methylpiperazin-1-yl)benzene-1,2-diamine (9) or 2-(4-(3,4-diaminophenyl)piperazin-1-yl)ethanol (10), $Na_2S_2O_5$, EtOH, 80 °C, 12 h, 55–60%.



Scheme 3 Reagents, conditions and yield. (a) $NaOH$, $THF-H_2O$, $p-TsCl$, 0 °C → rt, 6 h, 100%; (b) 1,4-dibromobutane, TBAI, 50% $NaOH$, rt, 12 h, 72%; (c) piperazine, K_2CO_3 , acetonitrile, rt, 6 h, 89%; (d) K_2CO_3 , acetone, 60 °C, 6 h, 70%; (e) $ZnCl_2$, $DMF-POCl_3$, 100 °C, 48 h, 50%; (f) 4-(4-methylpiperazin-1-yl)benzene-1,2-diamine (9) or 2-(4-(3,4-diaminophenyl)piperazin-1-yl)ethanol (10), $Na_2S_2O_5$, EtOH, 80 °C, 12 h, 45–55%.

Table 1 Dissociation constants (K_d) of the ligands with the preformed Hum₂₁ G4 DNA^a

Entry	Ligand	Dissociation constant, K_d ^a (μM) (Hum ₂₁ G4 DNA)	Hypochromicity ^a (%) (Hum ₂₁ G4 DNA)	n
1	M1	3.30 ± 0.2	17	2.9
2	D1	0.10 ± 0.001	26	2.0
3	D3	0.05 ± 0.001	17	2.4
4	M2	0.63 ± 0.04	40	2.5
5	D2	0.13 ± 0.01	37	1.9
6	D4	0.01 ± 0.001	43	2.0

^a Binding assays were performed with the preformed Hum₂₁ G4 DNA in 10 mM Tris-HCl (pH 7.4) having 0.1 M NaCl/KCl and 0.1 mM EDTA at 25 °C.

were adequately characterized by IR, ¹H, ¹³C NMR, mass spectrometry and elemental analysis as given in the Experimental section.

UV-vis absorption spectral titrations

The affinity of each ligand toward the preformed G4 DNA was investigated first using UV-vis absorption spectroscopy. Each ligand solution was titrated against progressively increasing concentrations of the G4 DNA in 10 mM Tris-HCl (pH 7.4) containing 0.1 M NaCl/KCl and 0.1 mM EDTA. All the titrations showed strong hypochromism in the ligand absorption band, suggesting the interaction between the chromophoric ligand with the nucleobases in the G4 DNA (ESI, Fig. S3–S5†).

The interaction between the ground states of the conjugated π -system of the ligand and the nucleobases in DNA probably decreased the extent of $\pi-\pi^*$ transition. The absorption data were converted into the Scatchard plot to determine the binding constant of each ligand with the G4 DNA following a reported protocol.¹⁸ Similarly, each ligand solution was titrated with duplex DNA (CT DNA and the telomeric duplex DNA), which showed a practically negligible extent of hypochromism, revealing the high selectivity of the ligands toward the G4 DNA over the duplex DNA (ESI, Fig. S3–S5†). The binding affinity of each ligand toward both forms of DNA is summarized in Table 1.

Fluorescence emission spectral titrations

All the ligands being aromatic with a π -conjugated skeleton showed intrinsic fluorescence emission properties. Upon excitation at the molecular absorption maxima (~320 or 350 nm) in a buffer, the ligands showed very low emission which could be possibly due to the collisional quenching of the excited singlet state by polar water molecules. Interestingly, addition of the preformed G4 DNA resulted in the increment in the fluorescence intensity even up to 5-fold followed by saturation (Fig. 2A and ESI, Fig. S6–S8†). The ligands arising from the association with the G4 DNA created a hydrophobic micro-environment to hide from the aqueous media, which resulted in the recovery of their intrinsic fluorescence. The enhancement

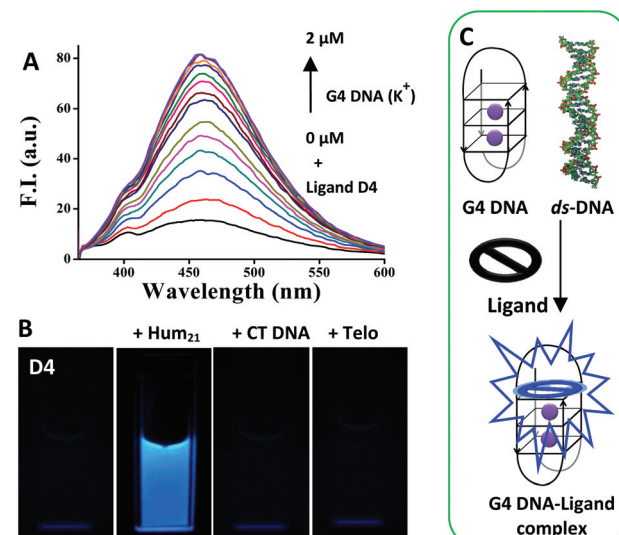


Fig. 2 (A) Fluorescence titrations of 0.8 μM ligand D4 in 10 mM Tris-HCl (pH 7.4) having 0.1 mM EDTA and 0.1 M KCl with the preformed Hum₂₁ G4 DNA. (B) Photographic fluorescence images of ligand D4 (20 μM) and ligand–DNA complexes (with 40 μM of Hum₂₁, CT DNA and Telo ds DNA) under UV light (>365 nm) in 10 mM Tris-HCl (pH 7.4) and 0.1 mM EDTA having either 0.1 M KCl (for the G4 DNA) or 0.04 M NaCl (for the CT DNA and the Telo ds DNA) and (C) a schematic representation of the process.

in the fluorescence intensity was more prominent in the case of the G4 DNA formed in the presence of K^+ ions than Na^+ . This may be due to the better association of the ligands with the K^+ -stabilized G4 DNA (ESI, Fig. S8A and C†). Among these ligands, the ones having hydroxyethyl substituted piperazines at the termini (**M2**, **D2**, and **D4**) showed higher fluorescence enhancements than the methyl substituted piperazines (**M1**, **D1**, and **D3**).

The dissociation constants calculated from the fluorescence spectral data³¹ (ESI, Table S1†) reveal that the dimeric ligands possess significantly higher binding affinities than their monomeric entities while the dimers containing piperazine in the linker (**D3** and **D4**) were found to be even superior to the corresponding ligands having hexaethylene glycol linkers (**D1** and **D2**). The ligand's efficient light-up probe behavior, which is selective for the G4 DNA as demonstrated from their fluorescence images (Fig. 2B and ESI, Fig. S9†) further exemplifies the superior binding affinities of the dimeric ligand **D4** toward the G4 DNA.

Fluorescent intercalator displacement assay

The G4 DNA-FID assays were undertaken to investigate each ligand's relative binding affinity toward the G4 DNA and selectivity over the duplex DNA. Thiazole orange (TO) which is a standard G4 DNA binding fluorophore has been chosen for the displacement assays.³² The extent of the TO displacement ability of a ligand from a preformed TO–G4 DNA complex corresponds to the decrease in the fluorescence intensity due

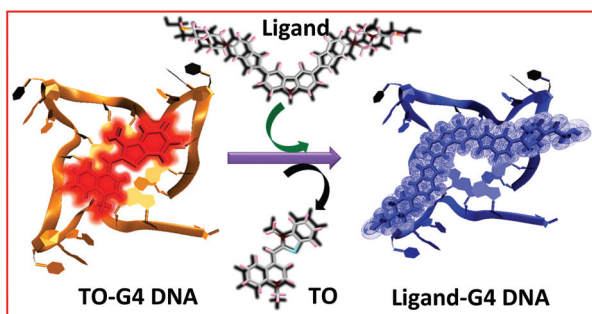


Fig. 3 A schematic representation of the G4 DNA-FID assay by a G4 DNA binding ligand.

Table 2 DC₅₀ values (ligand concentrations for the displacement of 50% of the bound TO from DNA) of the ligands as determined from fluorescent intercalator displacement assays^a

Ligand	DC ₅₀ (μM)	Ligand	DC ₅₀ (μM)
M1-G4 (K ⁺)	1.27 ± 0.09	D3-G4 (K ⁺)	0.31 ± 0.01
M2-G4 (K ⁺)	0.83 ± 0.03	D4-G4 (K ⁺)	0.27 ± 0.01
D1-G4 (K ⁺)	0.46 ± 0.03	D4-CT DNA (K ⁺)	>3.0
D2-G4 (K ⁺)	0.35 ± 0.02	D4-Telo ds (K ⁺)	>3.0

^a The G4 DNA-FID assays have been performed in 10 mM-Tris-HCl buffer (pH 7.4) containing 0.1 M KCl and 0.1 mM EDTA. Results are average of two independent experiments.

to TO upon binding (Fig. 3). All the ligands showed efficient TO displacement ability with significantly lower DC₅₀ (ligand concentrations for the displacement of 50% of the bound TO from DNA) values (ESI, Fig. S10,† Table 2) indicating their strong G-tetrad affinity. The ligands also exhibited high G4 DNA selectivity over the duplex DNA (CT DNA and Telo ds-DNA).

Circular dichroism spectroscopy

The DNA-ligand interactions were further probed using circular dichroism (CD) spectroscopy. The preformed G4 DNA was titrated against increasing ligand concentrations (prepared in KCl or NaCl buffer of pH 7.4). All the titrations showed enhancement in the CD intensity followed by saturation resembling the stabilization of the G4 DNA by the ligands (ESI, Fig. S11†).

Ligand induced G4 DNA structural alteration

The polymorphic nature of the human telomeric G-rich sequence in the presence of different monovalent ions like Na⁺, K⁺, NH₄⁺ and Li⁺ has been extensively studied and established either from NMR or from solved crystal structures.³³ The K⁺-stabilized mixed hybrid structure has the highest stability whereas Na⁺ can stabilize to a considerably lower extent.³⁴ The crystal structure and NMR solved structures suggest that in the presence of K⁺ ions the sequence d[5'-AG₃(T₂AG₃)₃-3']

adopts an intramolecular mixed hybrid structure whereas in the presence of Na⁺ ions it forms an intramolecular G-tetraplex stabilized by three stacked G-tetrads connected by two lateral loops and a central diagonal loop known as the antiparallel G-quadruplex.³⁵

The CD titrations of the preformed G4 DNA with the ligands show that all the ligands can stabilize the G4 DNA in their native form. It is believed that the telomeric G4 DNA remains in equilibrium with the single-stranded form. So it would be interesting to investigate whether the ligands have any significant effect on the formation of the G4 structure. We prepared the G4 DNA in 0.1 M KCl buffer along with the ligands in different concentrations. The CD spectra showed a gradual transformation in the CD signature with increasing ligand concentrations (Fig. 4 and ESI, Fig. S12†). The characteristic positive peaks at 293, 268, and 250 nm merged together to 263 nm with a shift of the trough from 235 nm to 242 nm, which is a specific CD signature due to the parallel G4 DNA formed by the human telomere sequences.¹⁸

There are only a handful of reports involving organic small molecules that induce topological transformations under physiological conditions.^{16,18,27,34,36} Though the existence of a telomeric parallel G4 DNA structure in K⁺ solution is rather unusual, such an organization may nevertheless possess much higher stability than the probable mixed hybrid G4 structure. The loops around the G-tetrads of K⁺-stabilized G4 DNA in solution state may inhibit the ready access of the planar ligands to the end-tetrads. On the other hand K⁺-stabilized G4 DNA has also been found to exist in the parallel structure in the crystalline state (PDB 1KF1) which has only sidewise loops.³⁵ Thus, the end-tetrads in 1KF1 may be entirely accessible to the tetrad targeting planar ligands. The presence of favorable binding sites may allow topological transformation of the G4 DNA in the presence of ligands. The presence of a ligand may further guide the telomere to fold in the thermodynamically more stable form of G4 DNA and justify the G4 DNA targeted approach to drug design.

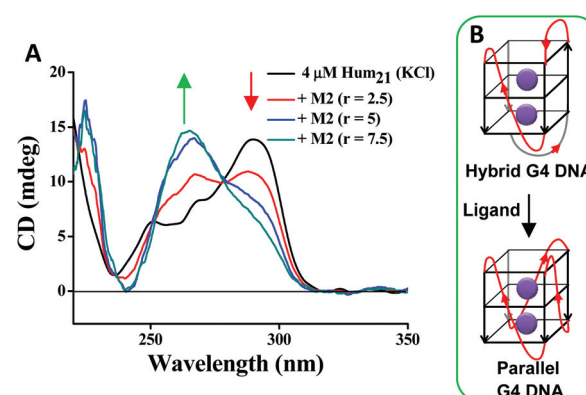


Fig. 4 (A) Formation of the G4 DNA in the presence of M2 in 10 mM Tris-HCl (pH 7.4) containing 0.1 M KCl and 0.1 mM EDTA and (B) a schematic representation of the process.

Thermal denaturation study

The thermal denaturation of DNA has been monitored by following the temperature-dependent changes in the CD spectra. CD spectroscopy provides a characteristic signature of the nucleobases in the DNA sequence as well as the conformation it adopts. Any change in the DNA conformation affects the position and amplitudes of the CD signal.³⁷ The diverse CD signatures of the G4 DNA formed in the presence of different stabilizing ions originate from the nature of folding and orientation of the nucleobases flanked from the glycosidic bonds. The G4 DNA structures formed in both Na⁺ and K⁺ ion environments afford a prominent characteristic peak at 293 nm whereas the G-quadruplexes formed in the presence of a ligand (in KCl buffer) showed a peak at 263 nm.

The thermal denaturation study has therefore been followed at a wavelength of either 293 nm or 263 nm according to the G4 DNA-ligand complex CD signature under investigation. The melting studies showed an elevation in the denaturation temperature of the G4 DNA upon complexation with the ligands (Fig. 5A and B and ESI, Fig. S13 and S14†). Interestingly, the present set of ligands showed greater stability toward the K⁺-stabilized G4 DNA than the G4 DNA stabilized by Na⁺ ions (Fig. 5C and D and ESI, Tables S2 and S3†). Moreover, the stability of the G4 DNA formed in the presence of a ligand is significantly higher than the ligand-DNA complex formed upon incubation with the preformed G4 DNA (Fig. 5C and D and ESI, Tables S2 and S3†).

The Na⁺-stabilized G4 DNA (PDB 143D) has a mixed anti-parallel and parallel stranded intramolecular structure with

three G-tetrads connected by one diagonal and two lateral (edgewise) TTA loops, which makes the G-tetrads inaccessible to the planar ligands.³⁵ On the other hand, K⁺-stabilized G4 DNA (PDB 2HY9) has two lateral loops and one sidewise loop.³⁵ Unlike possessing a rigid diagonal loop as in 143D, the dynamic nature of the lateral loops in 2HY9 keeps the G-tetrads accessible to the planar ligands. Thus, all the ligands showed better affinity toward the K⁺ ion stabilized G4 DNA form than the one stabilized by the Na⁺ ions. The higher denaturation temperatures of the G4 DNA in the presence of ligands were most likely due to the topological transformation from the hybrid to a more stable parallel structure (Fig. 4). The high thermal stability demonstrated the potency of the ligands as efficient G4 DNA binding and stabilizing agents. The melting curves of the preformed G4 DNA incubated with each ligand showed hysteresis in the reverse scan ($0.5\text{ }^{\circ}\text{C min}^{-1}$), possibly due to the formation of the G4 DNA structure in a kinetically slower process. However, the G4 DNA formed in the presence of each ligand in KCl buffer did not show any hysteresis in the reverse melting scan, possibly due the formation of the thermodynamically and kinetically more stable parallel G4 DNA structure (ESI, Fig. S13C†).

Electrophoretic mobility shift assay (EMSA)

The contribution of the ligands toward the formation of the G4 DNA was further investigated by an electrophoretic mobility shift assay (EMSA). We have used a 9-mer (Hum₉) human telomeric oligonucleotide having two stretches of GGG sequence d[5'-GGGTTAGGG-3'] where two such strands may associate to

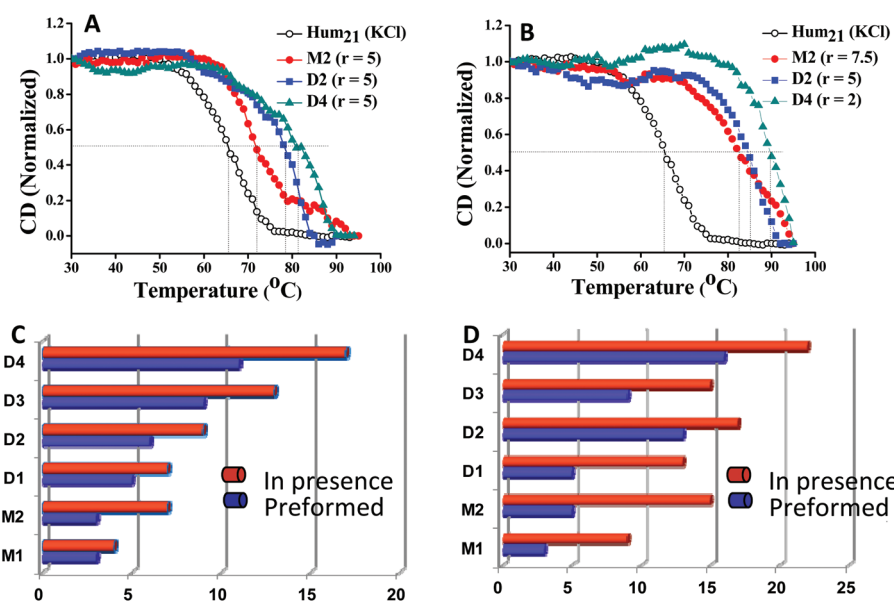


Fig. 5 Melting profiles of (A) G4 DNA incubated with various ligands (M2, D2 and D4) as monitored at a wavelength of 293 nm and (B) the G4 DNA formed in the presence of ligands (M2, D2 and D4) of specified concentration as monitored at a wavelength of 263 nm. Relative elevation in the G4 DNA melting temperature upon ligand incubation with either preformed G4 DNA or G4 DNA formed in the presence of ligand in 10 mM Tris-HCl (pH 7.4) containing 0.1 mM EDTA and (C) 0.1 M NaCl or (D) 0.1 M KCl. The ° results are average of two independent experiments and are within ±0.5 °C of each other.

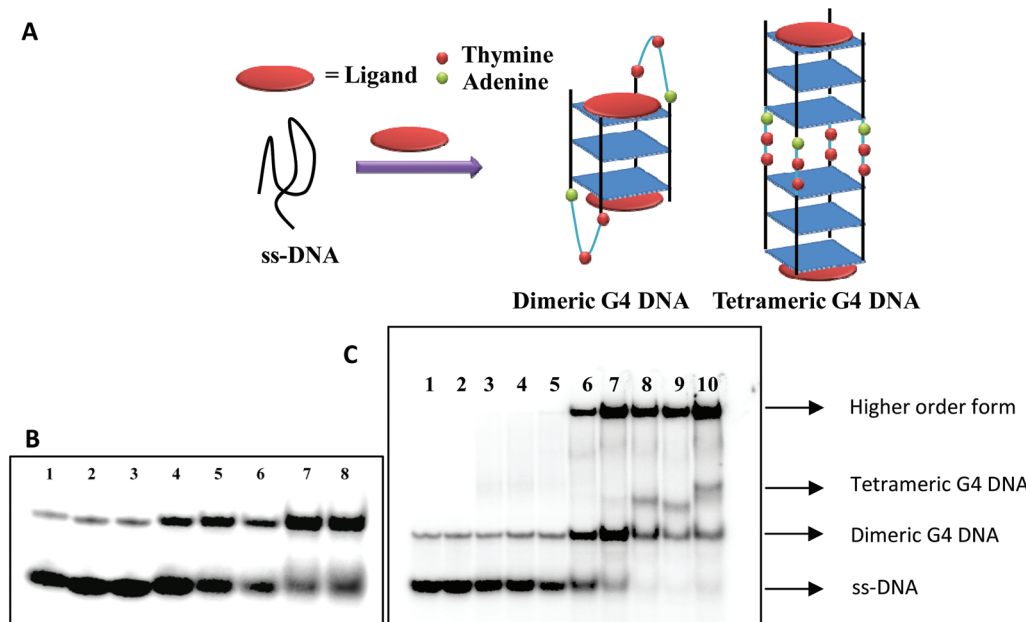


Fig. 6 (A) A schematic representation of the possible way of G4 DNA formation from the Hum9 DNA d[5'-GGGTTAGGG-3']. The electrophoretic mobility shift assay of 5'-GGGTTAGGG-3' (Hum9) DNA with increasing concentration of ligands. (B) Lane 1: DNA alone without KCl, lanes 2–8: DNA + **M2** ($r = 0, 1, 2, 4, 6, 8, 10$) in 50 mM KCl. (C) Lane 1: DNA alone without KCl, lanes 2–10: DNA + **D4** ($r = 0, 1, 2, 3, 4, 5, 6, 8, 10$) in 50 mM KCl.

form an intermolecular dimeric G4 DNA structure *via* Hoogsteen H-bonding among the guanine bases (Fig. 6A).^{38,39} Additionally, four such DNA strands can also combine together and form a tetrameric inter-molecular G4 DNA structure (Fig. 6A). To probe whether such DNA structures are formed in the presence of ligands or not, we performed experiments taking 10 μ M of DNA along with different ligand concentrations in 10 mM Tris-HCl buffer (pH 7.4) containing 50 mM KCl and 0.1 mM EDTA. We observed that with increasing ligand concentration, there was a sharp transition from the band of higher mobility to a band of lower mobility for both the ligands **M2** (Fig. 6B) and **D4** (Fig. 6C). The band with higher mobility corresponds to the single-stranded DNA whereas the less mobile one resembles the formation of an intermolecular dimeric G4 DNA of higher molecular weight.^{38,39} The ligand **M2** showed a transition of the ss-DNA to the dimeric G4 DNA whereas **D4** also generated a band corresponding to the tetrameric G4 DNA along with a higher order structure (Fig. 6C).³⁹ The existence of a higher order band may be attributed to the association of individual G4 DNA in the presence of a high concentration of a strong DNA binder like **D4**. The experiment therefore revealed the potential of such ligands as a G-quadruplex promoter and stabilizer even at a significantly lower K^+ concentration than the one under a more favorable physiological environment.

Telomerase inhibition assay (TRAP-LIG assay)

The over-expressed telomerase maintains the telomere length throughout the generations, and this is one mechanism by which the cells become immortal. Thus, the inhibition of telo-

merase activity through the G4 DNA stabilization has become a viable strategy in oncology. We have tested the present set of ligands for their anti-telomerase activity through a standard TRAP-LIG assay.^{40,41}

All the ligands were found to be highly potent telomerase inhibitors (Fig. 7A–D). The dimeric ligands were invariably found to be more efficient than the corresponding monomeric ligands. The IC₅₀ values showed a linear relationship with the extent of G4 DNA stabilizing abilities of the ligands (Fig. 7E and F). This manifests indirect but strong evidence of the telomerase inhibition mechanism through the G4 DNA stabilization.

In vitro cytotoxicity

The cell viabilities of ligand (**M2**, **D2**, and **D4**) treated cancer cells and normal cells were investigated in a MTT based short-term (72 h) cell viability assay. The ligand (5, 10, 15, and 20 μ M) treated HeLa (human cervical cancer), HT1080 (human fibrosarcoma), and A549 (human lung adenocarcinoma) cells showed a moderate decrease in the cell viabilities. The relatively higher IC₅₀ values (\sim 20 μ M) in a short-term assay indeed reveal the characteristics of a G-quadruplex selective DNA binding ligand over duplex DNA. On the other hand, the similar experiments performed in telomerase negative primary HFF (human foreskin fibroblast) cells⁴² did not show any noticeable loss in cell viability (Fig. 8A and ESI, Fig. S15†). The bright field images of the ligand treated cells corroborated the observations of cell viability assays where the differences in cellular morphology were clearly distinguishable in compari-

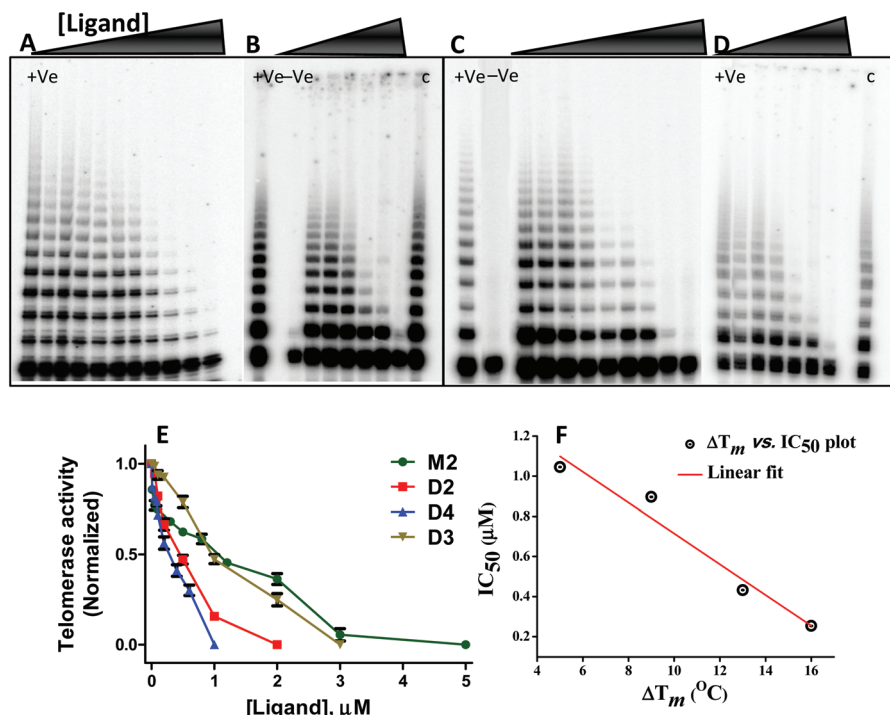


Fig. 7 The TRAP-LIG assay for ligands (A) **M2**, (B) **D2**, (C) **D4**, and (D) **D3**. Lane +ve: positive control; lane -ve: negative control; lane c: the final concentration of the solvent used for the dilutions and other lanes show the effect of increasing ligand concentrations in the range from 0.01 μ M to 5 μ M. (E) Telomerase activity against ligand concentration evaluated from the TRAP-LIG assay measured by UVI-Tech gel documentation station using UVI-Band Map software (version 97.04). (F) The plot of thermal stabilization against IC₅₀ values obtained from DNA denaturing experiments and the TRAP-LIG assay.

son with that of untreated cells, while no such events were observed in the ligand treated normal HFF cells (Fig. 8B).

The G4 DNA binding ligands which target the telomerase inhibition pathway require a sufficient time lag (≥ 8 days) to exhibit their activity for telomere shortening to occur.⁹ Therefore, the long-term (15 days) cytotoxicity experiments were also performed with a sub-cytotoxic ligand concentration (5 μ M). A significant cell growth inhibition was observed in the ligand treated cells in accord with their activity as observed in the short-term cell viability assay (Fig. 8C and D). This could be attributed to the cytotoxic events imparted by the telomerase inhibition due to the ligand mediated G4 DNA stabilization.

Apoptosis assay

The mode of cytotoxicity induced by the ligand treatments was investigated using Annexin V-FITC and PI dual staining assays.⁴³ HeLa cells, treated with 20 μ M of each of the ligand (**M2**, **D2**, and **D4**) for 48 h, showed the presence of a significant apoptotic population in accordance with their activity observed in MTT cell viability assays. The ligands **M2**, **D2**, and **D4** exhibited ~9%, ~15%, and ~35%, respectively, of early apoptotic populations after 48 h (Fig. 9A–D).

The effect of the ligand activity leading to cell death induced by apoptosis was also examined by PI nuclear counterstaining under fluorescence microscopy. The HeLa cells incubated with each ligand (48 h) showed the presence of

condensed and fragmented nuclei, which are characteristic of apoptotic cells (Fig. 9E–J and ESI, Fig. S16†). On the other hand, normal cells treated with each of the ligands did not exhibit any noticeable change in nuclear morphology under similar conditions (ESI, Fig. S17†). This observation seems to be quite evident for the cancer cell specific toxicity induced by apoptosis upon treatment with a ligand.

Cellular internalization

The cellular internalization of G4 DNA binding ligands was analyzed by means of fluorescence microscopy in cancer cell lines (HT1080 and HeLa) and normal cell lines (HFF) as well. The HeLa and HT1080 cells showed a prominent nuclear localization of the ligands after 24 h of incubation (Fig. 10 and ESI, Fig. S18†) where PI (propidium iodide) served as a nuclear counterstain. On the other hand, none of the ligands showed apparently distinct nuclear entry in normal HFF cells as was observed in the cancer cells (Fig. 11A and B).

We also looked at the cellular internalization of ligands in a co-culture environment of cancer (HT1080) and primary HFF cells.⁴⁴ The mixed cells in culture were incubated with ligand **D4** and observed under fluorescence microscopy. The bright field images of HT1080 and HFF cells helped to make a clearer analysis because of their apparently distinct morphologies. Interestingly, the nuclear distribution of the ligand was more distinct in HT1080 cells while HFF cells showed a significant

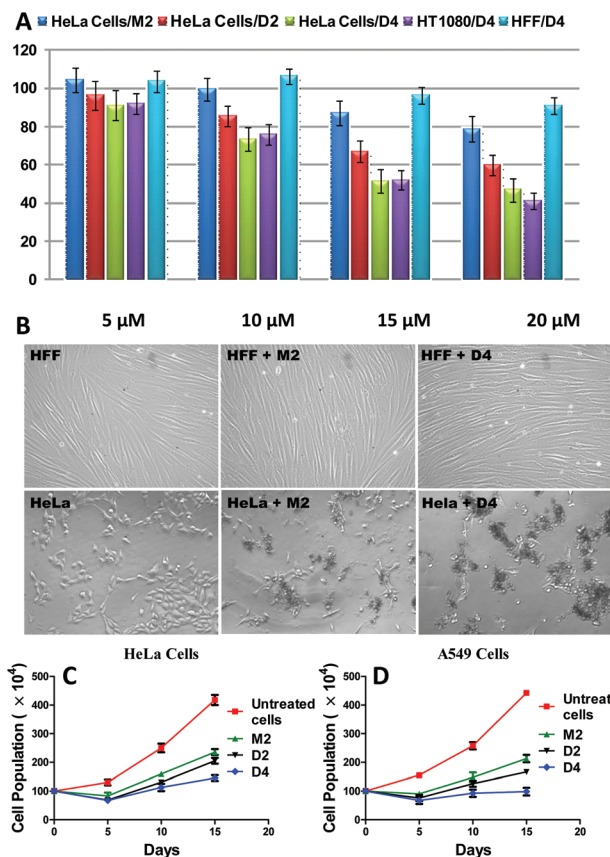


Fig. 8 Effect of ligands (M2, D2, and D4) on the cell viability after (A, B) short-term (72 h) and (C, D) long-term (15 days) exposure to different cancer and normal cells. The data represented are based on triplicates of each concentration treatment from at least three independent experiments.

cytoplasmic distribution. The ligand distribution pattern in co-culture is highlighted with the help of arrows (Fig. 11D). The observations made under co-culture experiments were nearly similar to that of cellular internalization patterns as shown in individually cultured cancer and normal cells.

Molecular dynamics simulation

The interaction between each ligand and the G4 DNA was further investigated with the help of Molecular Dynamics simulation studies. We performed studies considering the monomeric ligand **M2** and the most potent dimeric ligand **D4**. The optimized structures were converted into PDB using Open Babel software and docked with the parallel propeller-type X-ray resolved G4 DNA crystal structure (PDB 1KF1) using Auto-dock 4.0 software. The DNA-ligand complexes obtained from the docking studies were taken for the higher level of MD simulation using Amber 9 package software.⁴⁵ The MD simulations have been performed with a gradual reduction of the constraint following a procedure reported earlier (ESI†).¹⁸ The final production run of 6 ns without any constraint retained the DNA-ligand stable association reflected in the corresponding RMSD plot (ESI, Fig. S19C†).

The monomeric ligand efficiently stacked over the G-tetrad through the planar aromatic moiety covering three guanine bases (Fig. 12A). The end-piperazine moiety approached the groove interacting with the anionic phosphate backbone. For the dimer, one arm of the ligand interacts in the same fashion as the monomer targeting the end G-tetrad whereas the other arm interacts with the groove created by the T17-T18-A19 nucleobases (Fig. 12B and ESI, Fig. S19B†). The proximity of the linker piperazine with the G15 phosphate residue and the dual nature of the G-quadruplex recognition⁴⁶ enhanced the

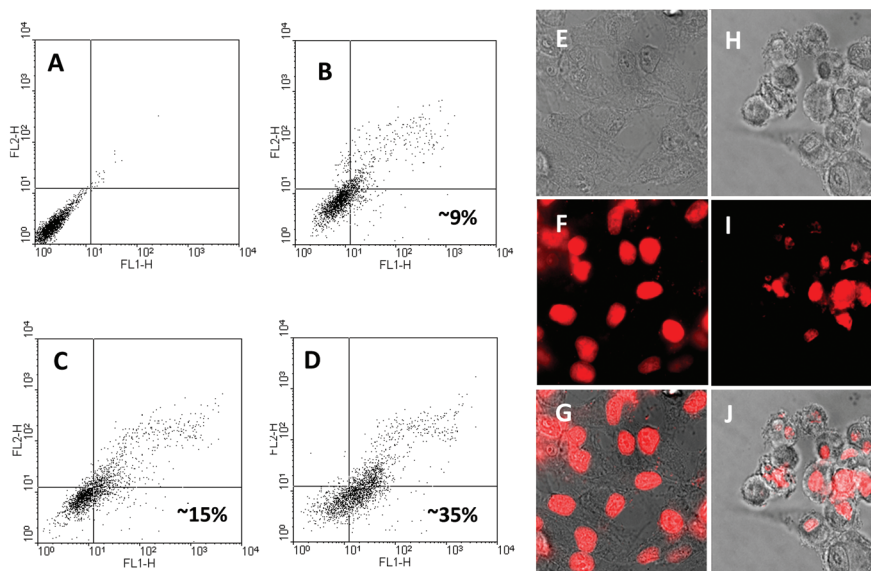


Fig. 9 Representative dot plots for Annexin-V and PI staining of untreated HeLa cells (A) and after incubation with ligands M2 (B), D2 (C), and D4 (D). The lower right quadrant represents early apoptotic cell population originated due to the Annexin V-FITC staining only. Representative bright field and fluorescence microscopic images of HeLa cells using PI as a nuclear counterstain. (E) Untreated HeLa cells and (H) cells treated with 20 μ M of the ligand D4 for 48 h. Panels E–G and H–J (top to bottom) represent bright field, PI nuclear counterstain (red) and overlay of the previous two images.

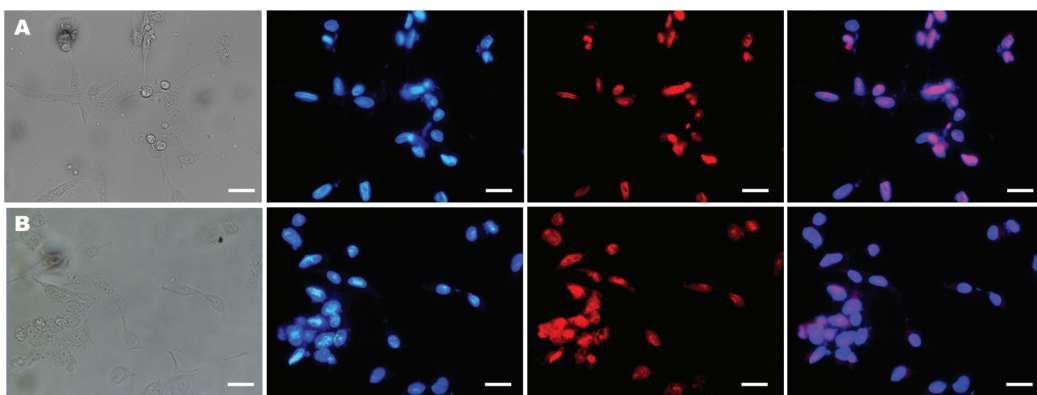


Fig. 10 Representative fluorescence microscopic images depicting cellular internalization of the ligand (A) M2 and (B) D4 in HT1080 cells at a concentration of 10 μM after 24 h. PI served as a nuclear counterstain. Panels A and B represent (left to right) bright field, ligand fluorescence (blue), PI nuclear counterstain (red) and overlay of ligand and PI fluorescence. Scale bar = 20 μm .

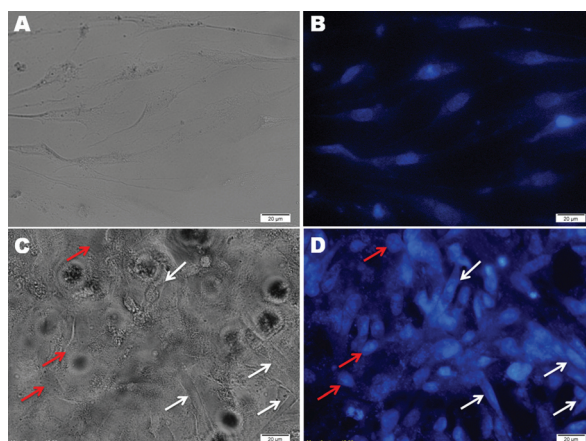


Fig. 11 Representative fluorescence microscopic images depicting cellular internalization of ligand D4 in HFF cells after incubation with 10 μM of D4 for 24 h and (C,D) HT1080 and HFF co-cultured cells after incubation with 10 μM of D4 for 24 h; red arrows indicate HT1080 cells and white arrows indicate HFF ones. Panels A and C (from left to right) represent bright field and ligand fluorescence (blue) respectively. Scale bar = 20 μm .

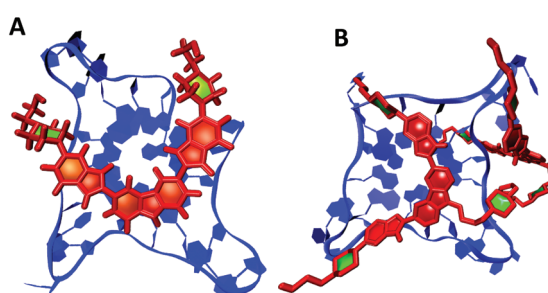


Fig. 12 MD simulated G4 DNA–ligand complexes for ligand (A) M2 and (B) D4 with 1KF1.

DNA–ligand interaction to a significant extent. The MD simulation results showed that the dimeric molecule interacts with 1KF1 more efficiently than the corresponding monomer.

Experimental methods

Synthetic procedures

3,6-Bis-(6-(4-methylpiperazin-1-yl)-1*H*-benzo[*d*]imidazol-2-yl)-9*H*-carbazole (1, M1). Freshly prepared (4-(4-methyl piperazin-1-yl)benzene-1,2-diamine) **9** (185 mg, 0.897 mmol) and the dialdehyde **13** (100 mg, 0.448 mmol) were mixed in 30 mL of ethanol. An aqueous solution of Na₂S₂O₅ (90 mg, 0.47 mmol) was added to the mixture and refluxed for 12 h. The reaction mixture was then cooled, filtered and evaporated to dryness under reduced pressure. The crude mass was then dissolved in methanol and precipitated by addition of ethyl acetate to it. Repetitive precipitation of the solid afforded the pure product as adjudged by TLC (5% MeOH/CHCl₃ on pre-coated silica gel). This was isolated as a brownish powder **1** (173 mg, 65%). ¹H NMR (400 MHz, DMSO-*d*₆): δ ppm 12.59 (br, 1H); 11.76 (br, 1H), 9.0 (s, 2H), 8.22 (d, *J* = 8, 2H), 7.65 (d, *J* = 8.4, 4H), 7.48 (s, 2H), 6.95 (s, 2H), 3.15 (s, 6H), 2.56 (s, 4H), 2.29 (s, 4H); ¹³C NMR (100 MHz, DMSO-*d*₆): δ ppm 172.12, 152.09, 147.09, 141.13, 124.74, 122.89, 121.8, 5, 118.55, 113.73, 111.80, 61.32, 59.20, 57.12, 52.68, 48.94, 21.18, 15.27; IR (KBr): 3422, 2970, 2870, 1635, 1442, 1289, 1241, 1185, 1143, 1009, 963, 897, 815 cm⁻¹; HRMS: *m/z* = 596.3247, calcd = 596.3250 [M + H]⁺; mp >300 °C. Anal. (calcd for C₃₆H₃₇N₉) C, 72.58; H, 6.26; N, 21.16; found: C, 72.31; H, 6.28; N, 21.2.

3,6-Bis-(6-(4-ethanol-2-yl)-piperazin-1-yl)-1*H*-benzo[*d*]imidazol-2-yl)-9*H*-carbazole (2, M2). Freshly prepared (2-(4-(3,4-diaminophenyl)piperazin-1-yl)ethanol) **10** (106 mg, 0.45 mmol) and the dialdehyde **13** (50 mg, 0.22 mmol) were mixed in 30 mL of ethanol. An aqueous solution of Na₂S₂O₅ (44 mg, 0.23 mmol) was added to the mixture and refluxed for 12 h. The reaction mixture was then cooled, filtered and evaporated to dryness under reduced pressure. The crude mass was then dissolved in methanol and precipitated by the addition of ethyl acetate to it. The repetitive precipitation afforded a pure product which was adjudged by TLC (5% MeOH/CHCl₃ on pre-coated silica gel). This was isolated as a brownish powder **2** (77 mg, 55%). ¹H NMR (400 MHz, DMSO-*d*₆): δ ppm 12.8 (br,

2H), 9.02 (s, 2H), 8.24 (d, J = 8.4, 2H), 7.66 (d, J = 8.4, 2H), 7.49 (t, J = 8.4, 2H), 7.04 (d, J = 9.2, 2H), 6.97 (d, J = 8.4, 2H), 4.8 (s, 2H), 3.67 (s, 8H), 2.95 (br, 8H), 2.81 (br, 8H); ^{13}C NMR (100 MHz, DMSO- d_6): δ ppm 172.12, 152.09, 147.09, 141.13, 124.74, 122.89, 121.85, 118.55, 113.73, 111.80, 61.32, 59.20, 57.12, 52.68, 48.94, 21.18, 15.27; IR (KBr): 3420, 2972, 2865, 1632, 1445, 1282, 1240, 1182, 1054, 945, 898 cm^{-1} ; HRMS: m/z = 656.3462, calcd = 656.3461 [M + H] $^+$; mp >300 °C. Anal. (calcd for $\text{C}_{38}\text{H}_{41}\text{N}_9\text{O}_2$) C, 69.6; H, 6.3; N, 19.22; found: C, 69.73; H, 6.33; N, 19.18.

1,17-Bis(9*H*-(3,6-bis(6-(4-methylpiperazin-1-yl)-1*H*-benzo[*d*]imidazol-2-yl)-carbazol)-9-yl)-3,6,9,12,15-pentaoxa-heptadecane (3, D1). Compound 3 has been synthesized from compound 17 following a similar procedure as described for compound 1. ^1H NMR (400 MHz, DMSO- d_6): δ ppm 12.87 (br), 9.06 (s, 4H), 8.30 (dd, J_1 = 1.2, J_2 = 8.8, 4H), 7.84 (dd, J_1 = 8.8, J_2 = 9.8, 4H), 7.48 (d, J = 7.6, 4H), 7.07 (s, 2H), 6.96 (d, J = 8.4, 8H), 4.90–4.7 (m, 4H), 4.15 (s, 2H), 3.91–3.74 (m, 14H), 3.62–3.56 (m, 18H), 3.27 (s, 22H), 2.35 (s, 6H); ^{13}C NMR (100 MHz, DMSO- d_6): δ ppm 15.12, 33.29, 43.10, 43.54, 43.99, 48.78, 53.77, 61.32, 68.88, 70.57, 110.54, 113.74, 118.39, 121.95, 121.99, 122.30, 122.48, 122.62, 124.64, 141.26, 141.38, 141.44, 141.58, 146.92, 151.89, 172.32; IR (KBr): 3512, 2937, 2821, 2699, 1636, 1457, 1289, 1240, 1219, 1190, 1145, 1010, 1024, 964, 897, 813 cm^{-1} ; HRMS: m/z = 703.3676, calcd = 703.3671 [M – 2CH₃] $^{2+}$; mp >300 °C. Anal. (calcd for $\text{C}_{84}\text{H}_{96}\text{N}_{18}\text{O}_5$) C, 70.17; H, 6.73; N, 17.54; found: C, 70.05; H, 6.75, N, 17.58.

1,17-Bis(9*H*-(3,6-bis(6-(4-(ethanol-2-yl)piperazin-1-yl)-1*H*-benzo[*d*]imidazol-2-yl)-9*H*-carbazole)-9-yl)-3,6,9,12,15-pentaoxa-heptadecane (4, D2). Compound 4 has been synthesized from compound 17 following a similar procedure as described for compound 2. ^1H NMR (400 MHz, DMSO- d_6): δ ppm 12.7 (br), 9.04 (s, 4H), 8.30 (dd, J_1 = 1.2, J_2 = 8.8, 4H), 7.85 (dd, J_1 = 8.8, J_2 = 9.8, 4H), 7.49 (d, J = 8.4 4H), 7.09–6.96 (m, 8H), 5.1 (br, 4H), 4.90 (s, 4H), 4.70 (s, 4H), 4.14 (t, J = 6, 4H), 3.92 (t, J = 5.8, 4H), 3.74 (m, 12H), 3.63 (m, 10H), 3.03 (s, 24H) 2.93 (s, 8H); ^{13}C NMR (100 MHz, DMSO- d_6): δ ppm 162.6, 162.5, 157.2, 152.3, 152.1, 135.4, 135.2, 135.1, 133.2, 133.1, 132.6, 132.3, 129.1, 128.9, 124.5, 121.2, 81.1, 79.5, 72.1, 68.9, 66.5, 62.56, 58.6, 54.3, 53.9, 21.2; IR (KBr): 3402, 3020, 2871, 1633, 1572, 1456, 1324, 1218, 1054, 835 cm^{-1} ; HRMS: m/z = 763.4062, calcd = 763.4064 [M – CH₂O] $^{2+}$; mp >300 °C. Anal. (calcd for $\text{C}_{88}\text{H}_{104}\text{N}_{18}\text{O}_9\text{H}_2\text{O}$) C, 67.07; H, 6.78; N, 16.0; found: C, 66.93; H, 6.8, N, 16.05.

1,2-Bis(2-(4-(9*H*-(3,6-bis(6-(4-methylpiperazin-1-yl)-1*H*-benzo[*d*]imidazol-2-yl)-carbazol)-9-yl)butyl)piperazin-1-yl)-ethoxy-ethane (5, D3). Compound 5 has been synthesized from compound 23 following a similar procedure as described for the synthesis of compound 1. ^1H NMR (400 MHz, CD₃OD): δ ppm 12.65 (br), 9.05 (s, 4H), 8.30 (t, J = 6.0, 4H), 7.80 (d, J = 8.4, 4H), 7.46 (d, J = 8.4, 4H), 7.04 (s, 4H), 6.94 (d, J = 7.6, 4H), 4.47 (s, 4H), 3.17 (s, 22H), 2.64 (s, 20H), 2.34 (s, 24H), 1.82 (s, 4H), 1.50 (s, 4H); ^{13}C NMR (100 MHz, DMSO- d_6): δ ppm 171.99, 151.66, 147.28, 141.13, 124.58, 122.40, 121.93, 118.41, 113.58, 110.06, 79.15, 69.48, 67.70, 61.22, 59.71, 56.70, 56.52, 54.36, 52.27, 51.88, 49.42, 48.57, 44.94, 42.39, 26.14, 22.96, 15.10;

HRMS: m/z = 1585.9728; calcd = 1585.9730 [M + H] $^+$; mp >300 °C. Anal. (calcd for $\text{C}_{94}\text{H}_{116}\text{N}_{22}\text{O}_2$) C, 71.18; H, 7.37; N, 19.43; found: C, 71.07; H, 7.39; N, 19.4.

1,2-Bis(2-(4-(4-(9*H*-(3,6-bis(6-(4-methylpiperazin-1-yl)-1*H*-benzo[*d*]imidazol-2-yl)-9*H*-carbazole)-9-yl)butyl)piperazin-1-yl)-ethoxyethane (6, D4). Compound 6 has been synthesized from compound 23 following a similar procedure as described for the synthesis of compound 2. ^1H NMR (400 MHz, CD₃OD): δ ppm 12.8 (br), 9.05 (s, 4H), 8.30 (d, J = 8.4, 4H), 7.82 (d, J = 8.4, 4H), 7.47 (d, J = 7.6 4H), 7.04 (s, 4H), 6.96 (d, J = 8, 4H), 4.76 (s, 4H), 4.50 (s, 6H), 3.63 (s, 12H), 3.22 (s, 22H), 2.86–2.50 (m, 36H), 1.83 (s, 4H), 1.54 (s, 4H); ^{13}C NMR (100 MHz, DMSO- d_6): δ ppm 173.8, 152.0, 147.3, 141.4, 139.1, 125.0, 122.5, 121.3, 118.7, 115.9, 114.3, 110.3, 101.1, 69.5, 66.9, 63.5, 62.6, 59.0, 57.0, 56.2, 56.1, 55.4, 52.5, 51.2, 51.0, 48.8, 44.8, 43.1, 42.5, 26.1, 22.4, 21.5, 15.0; IR (KBr): 3450, 2937, 2709, 1633, 1606, 1457, 1380, 1242, 1022, 960, 813, 722 cm^{-1} ; MALDI: m/z = 1706.015, calcd = 1706.015 [M + H] $^+$; mp >300 °C. Anal. (calcd for $\text{C}_{98}\text{H}_{124}\text{N}_{22}\text{O}_6\text{H}_2\text{O}$) C, 68.27; H, 7.37; N, 17.87; found: C, 68.17; H, 7.36; N, 17.91.

G-quadruplex formation

Hum₂₁ sequence, d[5'-G₃(T₂AG₃)₃-3'] was incubated in 10 mM Tris-HCl (pH 7.4), containing 0.1 M of the indicated salt and 0.1 mM EDTA, and the mixture was heated at 95 °C for 5 min and cooled slowly to room temperature over 24 h. The formation of G4 DNA was confirmed by their circular dichroic spectral signatures and melting profiles with that reported in the literature as well as by PAGE.²⁶

Electrophoretic mobility shift assay (EMSA)

The 9-mer telomeric DNA sequence d[5'-GGGTTAGGG-3'] was labeled with ³²P-ATP at the 5'-end and purified by Sephadex G-50 column followed by 15% PAGE. The required band was transferred into a centrifuge tube and eluted in TE buffer of pH 7.4 to obtain the labeled oligomer. The labeled DNA was then mixed with unlabeled ODN of identical sequence for further experiments. A 20 μL aliquot of 10 μM DNA in 10 mM Tris-HCl (pH 7.4) containing 50 mM KCl and 0.1 mM EDTA was mixed with different concentrations of a given ligand and heated to 95 °C for 5 min followed by slow cooling to rt over 24 h. An aliquot of 10 μL of this solution was mixed with 2 μL of gel loading dye (30% glycerol, 0.1% bromophenol blue, and 0.1% xylene cyanol) and loaded on a 15% polyacrylamide gel and electrophoresed for 8 h at 120 V at 4 °C in 0.5× running buffer (pH 7.4) containing 20 mM KCl. The gels were finally dried and visualized using a phosphorimager.

Cell viability assay

The cells were seeded in 96-well cell culture plates (15×10^3 per well) and grown for 24 h for the cells to adhere. The cells were then exposed to different concentrations of ligands or an equivalent volume of DMSO (0.1%) in the presence of 10% FBS. After 72 h of incubation, 20 μl of MTT (5 mg mL⁻¹) reagent was added to each well and incubated for another 4 h. The old medium was then removed and DMSO (200 μl) was

added to the wells. The readings were taken at 570 nm on an ELISA plate reader. The results reported are based on the triplicates of three independent experiments. Percentage (%) cell viability was calculated using the formula, % cell viability = $[(\text{FI}_{(570)} \text{ of treated cells} - \text{FI}_{(570)} \text{ of plain DMSO}) / (\text{FI}_{(570)} \text{ of untreated cells} - \text{FI}_{(570)} \text{ of plain DMSO})] \times 100$.

Long-term cell viability assay

In a typical long-term viability assay, $\sim 5.0 \times 10^4$ cells per well were grown in 6-well tissue culture plates and treated with a sub-cytotoxic concentration of (5 μM) or an equivalent of 0.1 volume% DMSO. The cells in untreated and ligand-treated wells were counted and re-seeded with half the population of the cells. This process was continued for a total of 15 days. Finally, cell population vs. time (days) plots were generated.

Annexin V-FITC and PI staining assay

An Annexin V-FITC and PI Apoptosis Detection kit (Sigma) were used to detect apoptosis in the ligand treated HeLa cells. In a typical experiment, cells were seeded at a 0.25 million cell population in 6-well cell culture plates. After 24 h, the cells were incubated with each ligand for 48 h at a final concentration of 20 μM . The cells were then thoroughly washed with DPBS buffer followed by trypsinization and resuspended in 1 \times binding buffer (HEPES buffer containing 0.14 M NaCl and 2.5 mM CaCl₂). Thereafter, Annexin V-FITC conjugate was added to each of the cell suspensions and incubated for ~ 10 min at room temperature keeping them protected from light. Then, each cell suspension was incubated with PI solution at a final concentration of 1 $\mu\text{g ml}^{-1}$ for ~ 5 min. Samples were then analyzed using a FACS Calibur flow cytometer (Becton-Dickinson). Data obtained from the flow cytometry were analyzed using WinMDI 2.9 software by considering gated cell population for the detection of % apoptotic cells.

Fluorescence microscopy

To visualize the cellular internalization of the ligands and apoptotic nuclei, fluorescence microscopic studies were performed. In a typical experiment, cells were cultured on a glass cover slip placed in 12 well cell culture plates. The cells were then treated with each ligand (24 h, internalization and 48 h, apoptosis) followed by washing thoroughly with DPBS. The cells were then fixed in 4% paraformaldehyde solution for ~ 10 min. Subsequently, cells were rinsed with DPBS and treated with 0.1% Triton-X-100 for ~ 5 min to permeabilize the cell membrane. Then the cells were washed with DPBS, and the glass cover slips were taken out and nuclei were counterstained with PI. Finally, the overstaining was removed by repeated washing with DPBS and then autoclaved in Milli-Q water, the cover slips were mounted on glass slides and observed under a fluorescence microscope (Olympus IX81).

For the co-culture experiments, HT1080 and HFF cells were mixed in an equal concentration of about 1.5×10^6 cells per ml and plated in 12-well cell culture plates. The next day, the cells were incubated with ligands for 24 h and the samples were processed as discussed above.

Conclusions

Herein, we report the design, syntheses and G4 DNA binding interactions of six carbazole based symmetric benzimidazole derivatives including two monomer and four corresponding dimeric ligands having different types of linkers. Spectroscopic and electrophoretic mobility analyses revealed the higher affinity and excellent selectivity of ligands toward G4 DNA over duplex DNA. The ligand's G4 DNA-specific fluorescence "turn-on" phenomenon helped in discriminating G4 DNA from duplex-DNA. Each of the ligands induced topological transformation of the K⁺-stabilized mixed-hybrid G4 DNA to a thermodynamically more stable parallel G4 DNA structure. The monomeric ligand **M2** could induce the formation of dimeric G4 DNA even at low K⁺ ion concentration. However, the dimeric ligand **D4** generated dimeric and tetrameric intermolecular G4 DNA structures from a 9-mer human telomeric DNA sequence. The ligands **M2**, **D2**, **D3**, and **D4** showed complete telomerase inhibition with IC₅₀ values in the sub-micromolar concentration range. Among all the molecules, the dimeric ligand **D4** showed highest telomerase inhibition activity (IC₅₀, 0.25 μM), which was higher by more than four times than that of the monomer. Interestingly, the activity shown by the dimeric bis-benzimidazole ligands presents them as the most potential telomerase inhibitors among all the bis-benzimidazole ligands reported to date.^{18,28,29} The absorption titration, CD spectroscopy, fluorescence titration and electrophoretic mobility analysis and the telomerase inhibition activity unambiguously demonstrated the superiority of the dimeric ligands over the monomeric ones. Among the dimeric molecules, the ligands with the piperazine moiety in the linker showed greater efficiency than the ligands with a neutral, hexaethylene glycol based spacer. The ligands demonstrated significant antiproliferative activity toward cancer cell lines without affecting the telomerase negative primary HFF cells. The ligand induced cytotoxicity was due to apoptosis as confirmed by Annexin V-PI dual staining (FACS) and PI nuclear counterstaining (fluorescence microscopy). The cellular internalization studies revealed a prominent nuclear localization of ligands in cancer cells in comparison with that of normal cells. The co-culture experiments revealed a distinct cellular distribution pattern of ligands toward cancer and normal cells. Concisely, we present a series of potent dimeric carbazole based bis-benzimidazole derivatives depicting the importance of linker design for improved G4 DNA binding and their prospects as telomere targeting putative anticancer drugs.

Acknowledgements

This work was supported by the J. C. Bose Fellowship, DST. S.B. B.M. acknowledges IISc for a Research Associate fellowship. The human foreskin fibroblast (HFF) cells were a kind gift from the Manipal University, Manipal.

Notes and references

- 1 R. J. O'Sullivan and J. Karlseder, *Nat. Rev. Mol. Cell Biol.*, 2010, **11**, 171–181.
- 2 A. Smogorzewska and T. D. Lange, *EMBO J.*, 2002, **21**, 4338–4348.
- 3 J. D. Griffith, L. Comeau, S. Rosenfield, R. M. Stansel, A. Bianchi, H. Moss and T. de Lange, *Cell*, 1999, **97**, 503–514.
- 4 D. Wynford-Thomas and D. Kipling, *Nature*, 1997, **389**, 551–552.
- 5 M. R. Lowden, S. Flibotte, D. G. Moerman and S. Ahmed, *Science*, 2011, **332**, 468–471.
- 6 J. Meyen, R. L. Ratliffe and R. K. Moyzis, *Proc. Natl. Acad. Sci. U. S. A.*, 1989, **86**, 7049–7053.
- 7 L. Armstrong, G. Saretzki, H. Peters, I. Wappler, J. Evans, N. Hole, T. V. Zglinicki and M. Lako, *Stem Cells*, 2005, **23**, 516–529.
- 8 A. M. Zahler, J. R. Williamson, T. R. Cech and D. M. Prescott, *Nature*, 1991, **350**, 718–720.
- 9 L. K. White, W. E. Wright and J. W. Shay, *Trends Biotechnol.*, 2001, **19**, 114–120.
- 10 A. K. Jain and S. Bhattacharya, *Curr. Pharm. Des.*, 2012, **18**, 1917–1933.
- 11 B. Maji and S. Bhattacharya, *Chem. Commun.*, 2014, **50**, 6422–6438.
- 12 A. M. Burger, F. Dai, C. M. Schultes, A. P. Reszka, M. J. Moore, J. A. Double and S. Neidle, *Cancer Res.*, 2005, **65**, 1489–1496.
- 13 R. Rodriguez, K. M. Miller, J. V. Forment, C. R. Bradshaw, M. Nikan, S. Britton, T. Oelschlaegel, B. Xhemalce, S. Balasubramanian and S. P. Jackson, *Nat. Chem. Biol.*, 2012, **8**, 301–310.
- 14 B. Maji and S. Bhattacharya, *Chimia*, 2013, **67**, 39–43.
- 15 S. A. Latt and G. Stetten, *J. Histochem. Cytochem.*, 1976, **24**, 24–33.
- 16 A. K. Jain, V. V. Reddy, A. Paul, K. Muniyappa and S. Bhattacharya, *Biochemistry*, 2009, **48**, 10693–10704.
- 17 G. Li, J. Huang, M. Zhang, Y. Zhou, D. Zhang, Z. Wu, S. Wang, X. Weng, X. Zhou and G. Yang, *Chem. Commun.*, 2008, 4564–4566.
- 18 B. Maji, K. Kumar, M. Kaulage, K. Muniyappa and S. Bhattacharya, *J. Med. Chem.*, 2014, **57**, 6973–6988.
- 19 S. E. Pierce, R. Kieltyka, H. F. Sleiman and J. S. Brodbelt, *Biopolymers*, 2009, **91**, 233–243.
- 20 W. Maneerat, T. Ritthiwigrom, S. Cheenpracha, T. Promgool, K. Yossathera, S. Deachathai, W. Phakhodee and S. Laphookhieo, *J. Nat. Prod.*, 2012, **75**, 741–746.
- 21 C. C. Chang, J. Y. Wu, C. W. Chien, W. S. Wu, H. Liu, C. C. Kang, L. J. Yu and T. C. Chang, *Anal. Chem.*, 2003, **75**, 6177–6183.
- 22 F. C. Huang, C. C. Chang, P. J. Lou, I. C. Kuo, C. W. Chien, C. T. Chen, F. Y. Shieh, T. C. Chang and J. J. Lin, *Mol. Cancer Res.*, 2008, **6**, 955–964.
- 23 M. P. Teulade-Fichou, C. Carrasco, L. Guittat, C. Bailly, P. Alberti, J. L. Mergny, A. David, J. M. Lehn and W. D. Wilson, *J. Am. Chem. Soc.*, 2003, **125**, 4732–4740.
- 24 P. Alberti, J. Ren, M. P. Teulade-Fichou, L. Guittat, J. F. Riou, J. Chaires, C. Helene, J. P. Vigneron, J. M. Lehn and J. L. Mergny, *J. Biomol. Struct. Dyn.*, 2003, **19**, 505–513.
- 25 Y.-T. Fu, B. R. Keppler, J. Soares and M. B. Jarstfer, *Bioorg. Med. Chem.*, 2009, **17**, 2030–2037.
- 26 A. De Cian, G. Cristofari, P. Reichenbach, E. De Lemos, D. Monchaud, M. P. Teulade-Fichou, K. Shin-Ya, L. Lacroix, J. Lingner and J. L. Mergny, *Proc. Natl. Acad. Sci. U. S. A.*, 2007, **104**, 17347–17352.
- 27 K. Iida, M. Tera, T. Hirokawa, K. Shin-ya and K. Nagasawa, *Chem. Commun.*, 2009, 6481–6483.
- 28 A. Paul, A. K. Jain, S. Misra, B. Maji, K. Muniyappa and S. Bhattacharya, *PLoS One*, 2012, **7**, e39467.
- 29 A. K. Jain, A. Paul, B. Maji, K. Muniyappa and S. Bhattacharya, *J. Med. Chem.*, 2012, **55**, 2981–2993.
- 30 D. A. Patrick, D. W. Boykin, W. D. Wilson, F. A. Tanious, J. Spychalaz, B. C. Bender, J. E. Hall, C. C. Dykstr, K. A. Ohemeng and R. R. Tidwell, *Eur. J. Med. Chem.*, 1997, **32**, 781–793.
- 31 S. Maiti, N. K. Chaudhury and S. Chowdhury, *Biochem. Biophys. Res. Commun.*, 2003, **310**, 505–512.
- 32 D. Monchaud, C. Allain, H. Bertrand, N. Smargiasso, F. Rosu, V. Gabelica, A. De Cian, J. L. Mergny and M. P. Teulade-Fichou, *Biochimie*, 2008, **90**, 1207–1223.
- 33 G. N. Parkinson, M. P. H. Lee and S. Neidle, *Nature*, 2002, **417**, 876–880.
- 34 A. Paul, B. Maji, S. Misra, A. K. Jain, K. Muniyappa and S. Bhattacharya, *J. Med. Chem.*, 2012, **55**, 7460–7471.
- 35 K. W. Lim, S. Amrane, S. Bouaziz, W. Xu, Y. Mu, D. J. Patel, K. N. Luu and A. T. Phan, *J. Am. Chem. Soc.*, 2009, **131**, 4301–4309.
- 36 X. Wang, J. Huang, Y. Zhou, S. Yan, X. Weng, X. Wu, M. Deng and X. Zhou, *Angew. Chem., Int. Ed.*, 2010, **49**, 5305–5309.
- 37 B. Maji, S. K. Samanta and S. Bhattacharya, *Nanoscale*, 2014, **6**, 3721–3730.
- 38 S. Bianco, C. Musetti, A. Waldeck, S. Sparapani, J. D. Seitz, A. P. Krapcho, M. Palumbo and C. Sissi, *Dalton Trans.*, 2010, **39**, 5833–5841.
- 39 G. Zagotto, A. Ricci, E. Vasquez, A. Sandoli, S. Benedetti, M. Palumbo and C. Sissi, *Bioconjugate Chem.*, 2011, **22**, 2126–2135.
- 40 J. Reed, M. Gunaratnam, M. Beltran, A. P. Reszka, R. Vilar and S. Neidle, *Anal. Biochem.*, 2008, **380**, 99–105.
- 41 A. D. Cian, G. Cristofari, P. Reichenbach, E. D. Lemos, D. Monchaud, M. P. Teulade-Fichou, K. Shin-Ya, L. Lacroix, J. Lingner and J. L. Mergny, *Proc. Natl. Acad. Sci. U. S. A.*, 2007, **104**, 17347–17352.
- 42 I. Naasani, F. Oh-Hashi, T. Oh-Hara, W. Y. Feng, J. Johnston, K. Chan and T. Tsuruo, *Cancer Res.*, 2003, **63**, 824–830.

- 43 P. Merle, B. Evrard, A. Petitjean, J.-M. Lehn, M. P. Teulade-Fichou, E. Chautard, A. D. Cian, L. Guittat, P. L. T. Tran, J. L. Mergny, P. Verrelle and A. Tchirkov, *Mol. Cancer Ther.*, 2011, **10**, 1784–1795.
- 44 Y. Song, W. Shi, W. Chen, X. Li and H. Ma, *J. Mater. Chem.*, 2012, **22**, 12568–12573.
- 45 D. A. Case, T. A. Darden, T. E. Cheatham III, C. L. Simmerling, J. Wang and R. E. Duke *et al.*, *Amber* 9, University of California, San Francisco, 2006.
- 46 N. Ranjan, E. Davis, L. Xue and D. P. Arya, *Chem. Commun.*, 2013, **49**, 5796–5798.